

# Multispectral Images and Panchromatic Remote Sensing Images Fusion Algorithm Based on Wavelet Transform

Xingyue Zhang<sup>1,\*</sup>, Mingju Chen<sup>1,2</sup>

<sup>1</sup>*School of Automation and Information Engineering, Sichuan University of Science & Engineering, Yibin, Sichuan, China*

<sup>2</sup>*Artificial Intelligence Key Laboratory of Sichuan Province, Sichuan University of Science & Engineering, Yibin, Sichuan, China*

*\*Corresponding Author.*

**Abstract:** Multispectral images and panchromatic remote sensing images carry incomplete spectral information, which reduces the application value of spectral images. The fusion of these two types of images can increase the amount of spectral information, highlight the features, and to a certain extent, make up for the shortcomings of the two when they exist separately. However, the existing fusion algorithms cannot solve the problem of spectral distortion well, so this paper proposes a fusion algorithm of multispectral images and panchromatic remote sensing images, through the low-frequency component of multispectral images and the low-frequency component of panchromatic remote sensing images to get the new low-frequency component by the weighted average operation, the high-frequency component of multispectral images and panchromatic remote sensing images high-frequency component to get the new high-frequency component by adopting the rule of great value fusion. The new low-frequency and high-frequency components are finally inverted by wavelet to get the final fused images. Experiments show that the fusion effect of this algorithm is better than other algorithms; especially it can make up for the defects such as spectral distortion or image chunking that exist in some fusion algorithms. Moreover, when the number of wavelet decomposition layers is 2, the fusion images obtained by this algorithm is of better quality.

**Keywords:** Image Fusion; Wavelet Transform; Multispectral Images; Panchromatic Remote; Sensing Images

## 1. Introduction

Spatial and spectral resolution are two critical indicators for assessing the quality of spectral images, directly determining the practical value of such images. High spatial resolution provides abundant spatial details, facilitating the identification of geometric features within the target area. High spectral resolution images offer rich spectral information, enhancing the ability to finely identify substances. However, due to limitations in imaging mechanisms, satellites struggle to acquire remote sensing images that simultaneously possess both high spatial and spectral resolutions. These two aspects have consistently been in a mutually constraining state.

Currently, the majority of satellites are capable of collecting single-channel panchromatic remote sensing images and multi-band multispectral images. Panchromatic remote sensing images, covering the entire visible light spectrum in the wavelength range of 0.38 to 0.76 micrometers, are composite images with high spatial resolution but weak representation of the colors of Earth's features. In contrast, multispectral images have lower spatial resolution and higher spectral resolution, carrying rich spectral information. Therefore, the fusion of multispectral and panchromatic remote sensing images is a crucial research direction in the field of remote sensing technology, which effectively fuses multispectral images with lower spatial resolution and panchromatic images with higher spatial resolution to generate images with both high spatial and spectral resolution<sup>[1]</sup>. This fusion technique holds significant importance in various domains such as image processing<sup>[2]</sup>, healthcare<sup>[3]</sup>, urban planning, and agriculture.

Common fusion algorithms for multispectral

and panchromatic remote sensing images can be broadly classified into four categories: pixel-based fusion methods [4], feature-based fusion methods [5], model-based fusion methods [6], and deep learning-based fusion methods [7]. Among them, pixel-based fusion methods include Intensity–Hue–Saturation (IHS) transform fusion algorithm [8], Principal Components Analysis (PCA) transform fusion algorithm [9], wavelet transform fusion algorithm [10], and others.

Based on wavelet transform, this paper will study the performance of wavelet fusion algorithm between different decomposition layers, and analyze and compare the fusion quality between the fusion algorithm in this paper and other common representative algorithm.

## 2. Fusion Algorithm Based on Wavelet Transform.

### 2.1 Theoretical Basis of Wavelet Transforms

Wavelet transform [11] can decompose an image into sub-bands of different scales and directions. Among these, the approximation sub-band represents the overall contour or background information of the image, while the detail sub-bands contain texture, edges, and other detailed information. Leveraging the multi-scale nature of wavelet transform and incorporating flexible fusion rules, the fusion of multispectral and panchromatic remote sensing images can effectively integrate information from different sources or with different characteristics. This process generates high-quality images that simultaneously possess spatial details and fused spectral information. The wavelet transform of an image primarily involves two processes: decomposition and reconstruction, and its principles are as follows.

First, the row vectors of the image are subjected to Discrete Wavelet Transformation (DWT) to obtain the low-frequency component L and the high-frequency component H in the horizontal direction. Then, DWT is applied to each column of these two components to obtain the low-frequency component in both horizontal and vertical directions, the low-frequency component in the horizontal direction and the high-frequency component in the vertical direction, the high-frequency

component in the horizontal direction and the low-frequency component in the vertical direction, and the high-frequency component in both horizontal and vertical directions. The reconstruction process is precisely the opposite of the decomposition process, wherein the transformed results undergo column-wise Inverse Discrete Wavelet Transform (IDWT), followed by row-wise IDWT. The specific principal diagram of wavelet transform is shown in Figure 1.

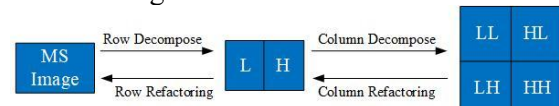


**Figure 1. Wavelet Transform Schematic Diagram**

Note: LL is the low frequency component in the horizontal and vertical directions, LH is the low frequency in the horizontal direction and the high frequency in the vertical direction, HL is the high frequency in the horizontal direction and the low frequency in the vertical direction, HH is the high frequency component in the horizontal and vertical directions

Additionally, according to the multi-scale characteristics of wavelet transform, it is possible to further decompose and reconstruct the obtained components during the transformation process. For example, Figure 2 illustrates a 3-level decomposition of the original image. This paper will also explore the impact of different decomposition levels on the performance of the fused image.



**Figure 2. Results of Original Image 3-level Wavelet Decomposition**

### 2.2 Fusion Steps Based on Wavelet Transform

The flow chart of the algorithm proposed in this paper is shown in Figure 3 below, and the specific steps are as follows.

(1) Wavelet forward transform. Performing wavelet decomposition on the multispectral

image (MS) and the panchromatic remote sensing image (PAN) separately yields their corresponding low-frequency components, MSL and PANL, and high-frequency components, MSH and PANH. Here, MSL and MSH represent the low-frequency and high-frequency components of the multispectral image MS, while PANL and PANH represent the low-frequency and high-frequency components of the panchromatic remote sensing image PAN.

(2) Frequency domain fusion. The low-frequency components, MSL and PANL, obtained from decomposition are subjected to weighted averaging to obtain the low-frequency component, L1. The high-frequency components, MSH, and PANH, are processed using the maximum value fusion rule to obtain the high-frequency component, H1.

(3) Wavelet inverse transform. Applying the wavelet inverse transform to the low-frequency component L1 and the high-frequency component H1 results in the fused image MS1.

The algorithm flowchart of this paper is as follows:

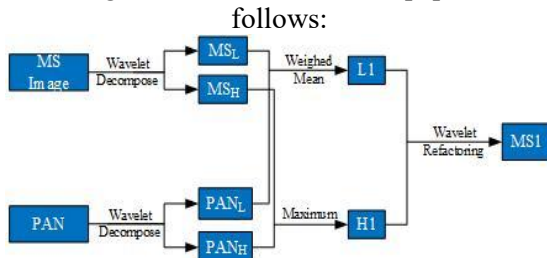


Figure 3. Algorithm Flow Chart

### 3. Experiment Results and Analyses

#### 3.1 Experimental Data

This paper selects land features with distinct characteristics and abundant resources in their respective regions as experimental data, as illustrated in Figure 4. The data consists of urban residential images, including streets, houses, roads, and vegetation. The data will be used to study the performance of the fusion algorithm between the layers of wavelet decomposition and to compare the performance of the fusion algorithm based on wavelet transform with several representative fusion algorithms.

#### 3.2 The Performance Comparison of Wavelet Fusion Algorithms among Different Decomposition Levels

This paper investigates the performance of

wavelet fusion algorithms across different decomposition levels. According to the experimental image size selected in this paper and the wavelet decomposition layer number rule ( $L=2^N$ , where L is the image size and N is the decomposition layer number), the number of decomposition layers in this paper are set at 2, 3, 4, and 5 layers. The specific experimental results and relevant analysis are presented below.

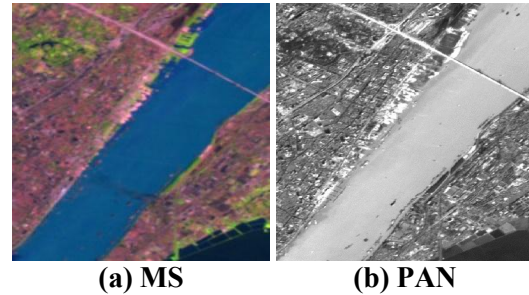


Figure 4. The Experimental Data

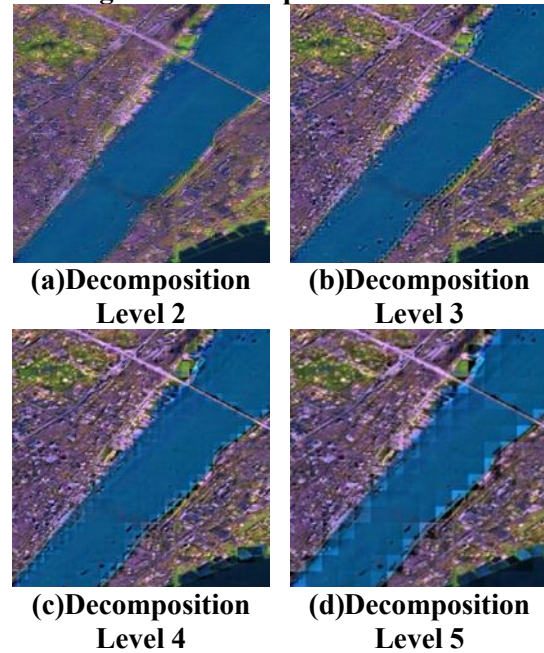


Figure 5. The Fusion Result of Different Decomposition Layers

Note: Figures a, b, c and d represent the fusion images corresponding to the decomposition layers of 2, 3, 4 and 5.

From Figure 5, it is evident that the visual effect of the image with a decomposition level of 3 in experimental data (b) is poor, with the image appearing blurry and lacking clear texture details. Image (a) has moderate brightness, and compared to image (b), it is clearer with a significantly enhanced spatial information preservation capability. However, images (c) and (d) exhibit distortion, with image (d) particularly suffering from severe

spectral distortion. Preliminary speculation suggests that the fusion effect of images with a decomposition level of 2 is better.

### 3.2.1 Objective Evaluation

The objective evaluation of fusion effects selects mutual information [12], peak signal-to-noise ratio [13], root mean square error [14], structural similarity [15], similarity coefficient [16], and information entropy [17] as evaluation metrics for fusion results. The root means square error closer to 0 is better and the structural similarity closer to 1 is better.

**Table 1. Objective Evaluation Results**

	Entropy	RMSE	PSNR	SSIM	SC	MI
W2-2	7.1659	<b>0.3985</b>	<b>22.1264</b>	<b>0.9999</b>	0.9980	<b>1.2202</b>
W2-3	7.2815	0.6101	20.2770	0.9998	0.9980	0.9673
W2-4	7.3733	0.7652	19.2928	0.9998	<b>0.9981</b>	0.8199
W2-5	<b>7.4492</b>	0.8987	18.5945	0.9998	0.9980	0.6925

Note: The optimal data is shown in bold.

The following information can be inferred from the data in Table 1:

(1) Entropy: The fusion image W2-5 with a wavelet decomposition level of 5 has the highest information entropy of 7.4492, followed by the fusion image W2-4 with a decomposition level of 4, and then the fusion image W2-3. According to the definition of information entropy, this indicates that the fusion image W2-5 with a decomposition level of 5 contains a larger amount of information, suggesting better fusion performance.

(2) Root Mean Square Error (RMSE): The fusion image W2-2 with a wavelet decomposition level of 2 has the smallest RMSE of 0.3985, while the fusion image W2-3 with a decomposition level of 3 has an RMSE of 0.6101, followed by W2-4 and W2-5. Therefore, the fusion image W2-2 with a decomposition level of 2 exhibits the strongest capability in preserving spatial detail information from the reference image.

(3) Peak Signal-to-Noise Ratio (PSNR): The fusion image W2-2 with a wavelet decomposition level of 2 has the most ideal PSNR value, which is 22.1264. The fusion image W2-3 with a PSNR of 20.2770, then W2-4, and finally W2-5 with the lowest PSNR. Hence, the distortion in the fusion image W2-2 with a decomposition level of 2 is relatively low, indicating higher image quality.

(4) Structural Similarity (SSIM): The fusion image W2-2 with a wavelet decomposition level of 2 has the most ideal structural

similarity coefficient of 0.9999. The structural similarity values for decomposition levels 3, 4, and 5 are all the same, at 0.9998, with a difference of 0.0001 from W2-2. Therefore, the structural difference between the fusion image W2-2 with a decomposition level of 2 and the reference image is smaller.

(5) Similarity Coefficient (SC): The fusion image W2-4 with a wavelet decomposition level of 4 has a similarity coefficient of 0.9981, while the similarity coefficients for other decomposition levels are all the same at 0.9980. Thus, the fusion image W2-4 with a decomposition level of 4 is more similar to the reference image, with lower distortion.

(6) Mutual Information (MI): The fusion image W2-2 with a wavelet decomposition level of 2 has the highest mutual information value of 1.2202, followed by W2-3 and then W2-4. Hence, the fusion image W2-2 with a decomposition level of 2 exhibits a stronger correlation with the reference image, indicating higher image quality.

In conclusion, it can be observed that the fusion image with a wavelet decomposition level of 2 obtains the most ideal objective data, resulting in the best image quality. Therefore, subsequent analysis will compare this fusion image with images obtained from other fusion algorithms to comprehensively evaluate the strengths and weaknesses of this algorithm.

### 3.3 The Performance of The Proposed Algorithm Is Compared with Other Fusion Algorithms

In this paper, the fusion performance of wavelet transforms based fusion algorithm, principal component (PCA) fusion algorithm, histogram matching based hue saturation (GIHS) fusion algorithm and hue saturation (IHS) fusion algorithm will be compared and analyzed. Specific experimental results and correlation analysis are as follows:

#### 3.3.1 Subjective Assessment

From Figure 6, it can be observed that image (a) has moderate brightness, but the details of the image are not sufficiently complete, and the boundary between the river and the bank is not clear. Image (b) has an overall color that is too bright, slightly dazzling to the eyes. Conversely, image (c) is quite the opposite, with an overall dark hue, although the colors of the forest and vegetation are particularly noticeable, the image as a whole is somewhat

blurry. Image (d) presents complete scene information, handles texture details well, has a stronger ability to preserve spatial information, and highlights geographic features more prominently. Therefore, the fusion algorithm proposed in this paper has better visual effects and higher image quality.

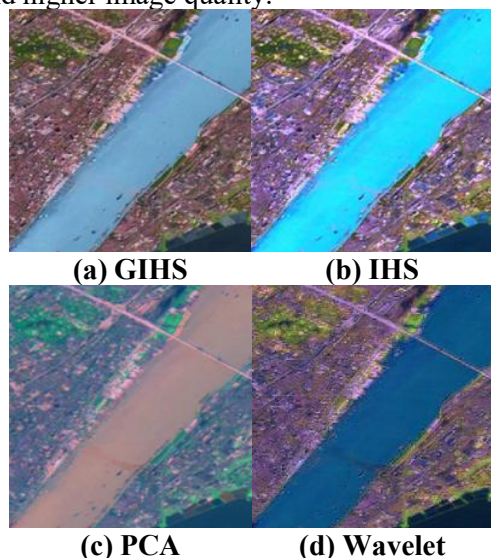


**Figure 6. The Results of Different Fusion Algorithms**

### 3.3.2 Objective Evaluation

The objective evaluation results of fusion images obtained by different fusion algorithms are shown in Table 2.

**Table 2. Objective Evaluation Results**

	Entropy	RMSE	PSNR	SSIM	CC	MI
MS	6.9144	—	—	—	—	—
PAN	7.3714	7.2045	9.5548	0.9933	0.9981	0.8522
GIHS	7.3581	2.7371	13.7579	0.9964	0.9981	0.8613
IHS	7.5449	4.8452	11.2777	0.9962	0.9981	0.9116
PCA	6.8580	3.7395	12.4026	0.9984	0.9981	1.1982
Wavelet	7.1659	0.3985	22.1264	0.9999	0.9980	1.2202

Note: The optimal data is shown in bold.

From Table 2, it can be observed that the Information Entropy of the IHS fusion algorithm is 7.5449, not only higher than the fusion algorithm adopted in this paper but also greater than several other fusion algorithms. This indicates that, to some extent, the IHS fusion algorithm performs better in processing the images of Experiment 2 compared to other algorithms. It may contain more information from the reference image, leading to potentially better quality in the fused image, highlighting a certain disadvantage of the fusion algorithm proposed in this paper. In addition to information entropy and similarity

coefficients, the various objective evaluation indicators of the wavelet fusion algorithm employed in this paper are superior to several other algorithms, especially the PSNR value, which reaches 22.1264. This indicates a stronger spatial preservation capability of the image and better quality in the fused image.

To sum up, it can be seen that the objective data of the wavelet fusion algorithm adopted in this paper is the most ideal, the quality of the fusion image is the best, the detailed control and differentiation of ground features presents a good visual effect, and can solve the problems of other algorithms such as spectral distortion and image blurring.

## 4. Conclusion

This study investigates the impact of the decomposition level of wavelet transform on the fusion performance of multispectral images and panchromatic remote sensing images. It was found that when the decomposition level is too low, the fused image tends to be blurry with overlapping texture details. On the other hand, when the decomposition level is too high, the fused image may exhibit spectral distortion and other artifacts. In this study, it was observed that the fusion image quality is optimal when the decomposition level is set to 2, resulting in a clearer and more defined image. Compared to several other algorithms, the algorithm proposed in this paper demonstrates certain advantages in both subjective evaluation and objective data. It effectively enhances spatial resolution while maintaining spectral characteristics, addressing issues such as spectral distortion, unclear texture details, and indistinct geographic features in images. The algorithm efficiently fuses multispectral images with panchromatic remote sensing images, resulting in images with high spectral and spatial resolutions. Undoubtedly, the fusion technology of multispectral and panchromatic remote sensing images is progressing towards greater intelligence, efficiency, and precision. The algorithm presented in this paper still has room for improvement, and future work will consider additional datasets to enhance its applicability or explore more effective fusion algorithms.

## Acknowledgments

This research was funded by the Natural

Science Foundation of Sichuan (grant number 2023NSFSC1987).

## References

- [1] Gemine V. Multispectral and hyperspectral image fusion in remote sensing: A survey. *Information Fusion*, 2023, 89405-417.
- [2] Chen M, Yi S, Lan Z, et al. An Efficient Image Deblurring Network with a Hybrid Architecture. *Sensors*, 2023, 23 (16).
- [3] Mingju C, Sihang Y, Mei Y, et al. UNet segmentation network of COVID-19 CT images with multi-scale attention. *Mathematical biosciences and engineering: MBE*, 2023, 20 (9): 16762-16785.
- [4] Yingqing H, Zhan Y, Xiaoyu J, et al. Performance Enhanced Elemental Array Generation for Integral Image Display Using Pixel Fusion. *Frontiers in Physics*, 2021, 9.
- [5] Ruizhe W, Wang X. Adaptive Enhancement Algorithm of High-Resolution Satellite Image Based on Feature Fusion. *Journal of Mathematics*, 2022.
- [6] Palubinskas. Model-based view at multi-resolution image fusion methods and quality assessment measures. *International Journal of Image and Data Fusion*, 2016, 7 (3): 203-218.
- [7] Yufei W, Chengchao Q, Qinglei D. Target recognition of heterogeneous fusion images based on improved YOLO model deep learning algorithm. *Journal of Physics: Conference Series*, 2022, 2170 (1).
- [8] Remote Sensing; Findings from Chongqing University of Posts and Telecommunications Broaden Understanding of Remote Sensing (Model-based Variational Pansharpening Method with Fast Generalized Intensity-hue-saturation). *Journal of Technology*, 2019.
- [9] Gunnam S, Bellamkonda S, Hari R M P, et al. Fusion of hyperspectral and multispectral images based on principal component analysis and guided bilateral filtering. *International Journal of System Assurance Engineering and Management*, 2022, 15 (1): 439-448.
- [10] Wavelet Research; Findings in Wavelet Research Reported from Sri Ramakrishna Institute of Technology (Hyperspectral image compression using hybrid transform with different wavelet-based transform coding). *Journal of Technology*, 2020.
- [11] Dahui L, Qi F, Jianzhao C, et al. Research on Target Detection Algorithm of Radar and Visible Image Fusion Based on Wavelet Transform. *Tehnički vjesnik*, 2020, 27 (5): 1563-1570.
- [12] Harmeet K, Satish K, Kuljinder B, et al. Multi-modality medical image fusion using cross-bilateral filter and neuro-fuzzy approach. *Journal of Medical Physics*, 2021, 46 (4): 263-277.
- [13] Chen M, Duan Z, Li L, et al. A Two-Stage Image Inpainting Technique for Old Photographs Based on Transfer Learning. *Electronics*, 2023, 12 (15).
- [14] Xianghai W, Xinying W, Ruoxi S, et al. MCT-Net: Multi-hierarchical cross transformer for hyperspectral and multispectral image fusion. *Knowledge-Based Systems*, 2023, 264.
- [15] Ahmed J B, Lianfang T, Qiliang D, et al. An Improved Infrared and Visible Image Fusion Using an Adaptive Contrast Enhancement Method and Deep Learning Network with Transfer Learning. *Remote Sensing*, 2022, 14 (4): 939-939.
- [16] Zhibo W, Youqiang D, Zengchen Y, et al. Semi-Supervised Support Vector Machine for Digital Twins Based Brain Image Fusion13; *Frontiers in Neuroscience*, 2021, 15705323-705323.
- [17] I S I, A M M, S G E. Multimodal medical image fusion algorithm based on pulse coupled neural networks and nonsubsampling contourlet transform. *Medical biological engineering computing*, 2022, 61 (1).